Applications of the LS3DF method in CeSe/CdS core/shell nano structures

Zhengji Zhao, *NERSC and* **Lin-Wang Wang**,
Computational Research Division, Lawrence Berkeley National Laboratory

ABSTRACT: *The Linear Scaling 3 dimensional fragment (LS3DF) method is an O(N) ab initio electronic structure method for large scale nano material simulations. The main idea of this approach is divide-and-conquer, and the heart of this method is the novel patching scheme that effectively cancels out the artificial boundary effect, which exists in all divide-and-conquer schemes. This method has made ab intio simulations of the thousands-atom nano systems tractable in terms of simulation time, while pertaining essentially the same accuracy as the direct calculation methods. The LS3DF method has won the Gordon Bell Prize in SC 2008 for its algorithmic achievement. We have applied this method to study the electronic structures and the internal electric filed in the asymmetric CdSe/CdS core/shell nano structures, which has potential applications for the electronic devices and solar cells.*

KEYWORDS: performance, *O(N)*, electronic structure, CdSe/CdS, asymmetric core/shell nano structure

1. Introduction

Nano structures have wide applications in the biological imaging, light emitting diodes, solar cells, and other electronic devices. The sizes of the nano structures are so small that they have very different electronic and optical properties from those of bulk materials, which have a strong dependence on the sizes of the nano structures (quantum confinement effect). Nevertheless, to study the properties of nano structures, one needs do *ab initio* calculations on the systems containing 1,000 to 100,000 atoms, which are too large for the direct *ab intio* methods to simulate. Despite the increasing availability of the computer processors, the direct methods have been applied to systems with one or two thousand atoms at most [1]. This is because even the simplest *ab initio* methods - the density functional theory (DFT) methods under the local density approximation (LDA), are computationally expensive, scaling as $O(N^3)$, where N is the size of the system. In addition, due to the communication bottleneck the parallelization of the direct LDA methods might have a limit in the order of 10,000 processors [1]. In reality, the most widely used direct LDA code, VASP, is difficult to scale to thousands of processors. Therefore, both the computational costs and the limit on parallelization call for a change in the direct $O(N^3)$ algorithm. The $O(N)$ methods are required to simulate nano structures. Over the past decade, many $O(N)$ methods have been developed [2]. These approaches can be classified to three main categories, the local orbital methods [3-4], the truncated D-matrix methods [5-6], and the divide and conquer methods [7]. While these methods have been able to successfully cut down the computational cost and have been applied to many larger systems, there exist some fundamental technical issues that are difficult to overcome. For example, in the commonly used local orbital methods, there exist extraneous local minima in the total energy functional, which make the total energy minimization difficult (convergence problem). This is due to constraining the wave functions on the local orbital manifold. Special methods and algorithms have been devised to overcome these problems [4]. Moreover, the overlap between neighbouring local orbitals has made these methods difficult to scale to the large number of processors. Some technical issues in the truncated density matrix methods (widely used in quantum chemistry) and the existing

divide and conquer methods have been discussed in more detail in Ref. [9]. As a summary about the previous *O(N)* methods, on top of some fundamental technical issues, the main challenge in these methods is to scale the codes to tens of thousands of computer processors while preserving the *ab intio* accuracy.

Recently we have developed a new *O(N)* method, the linearly scaling 3 dimensional fragment (LS3DF) method [8,9]. It is a divide and conquer method. It scales to tens of thousands of computer processors, and yields essentially the same results as the direct LDA methods. The code has been run on Cray XT3/XT4 at National Energy Research Scientific Computing Center (NERSC) at Lawrence Berkeley National Laboratory, Cray XT4/XT5 at National Center for Computational Sciences (NCCS) at Oak Ridge National Laboratory, and Blue Gene/P at Argonne Leadership Computing Facility (ALCF), and has shown the linear speedup upto the maximum available numbers of processors on all three supercomputers. It has reached 442 TFlops running on 147,456 processors on the Cray XT5 (Jaguar at NCCS) [10]. The largest number of processors on which it has been run on is 163,840, and the largest physical system it has been applied to contains 36,000 atoms.

In this paper, we will present the LS3DF method, focusing on its parallel performance. Then we will apply the LS3DF method to study the electronic structures of the asymmetric CdSe/CdS core/shell nanorods, which have potential applications in the solar energy conversions. We will present the computational details to demonstrate how the LS3DF method is used to solve interesting physics problems.

2. The LS3DF method

2.1 Formalism

The LS3DF method is based on the near-sightedness of quantum mechanical effects [11]. The total energy of a system can be split into the classical electrostatic energy and the quantum mechanical energy (kinetic energy and exchange correlation energy). The electrostatic interaction is long-ranged, therefore the electrostatic energy must be calculated by globally solving the Poission equation. But the quantum mechanical effect is short-ranged, therefore it can be solved locally, and then the quantum mechanical energy for the whole system can be obtained by combining the locally calculated quantum energies. In our LS3DF method, we divide a large system into small pieces (fragments), and independently calculate each fragment, then patch them together to obtain the total energy and the total charge density for the whole system. As all other divide and conquer methods, the artificial boundary effect due to the division of the system must be dealt with. The heart of the LS3DF method is a novel patching scheme that effectively cancels out the artificial boundary effect. Figure 1 and 2 illustrate our division and patching scheme using a 2D example for simplicity. In Figure 1 a periodic super cell is divided into 4x4 pieces. At each fragment grid point *(i,j)*, we introduce 4 fragments (along right-upper direction) with different sizes, 1x1, 2x1, 1x2 and 2x2. And then all fragments at all fragment grid point *(i,j)*, (*i=1,…,4; j=1,…,4*) will be calculated independently using a direct LDA method, eg., PEtot [12], a planewave pseudo potential LDA code. Then, the fragments will be summed up according to the patching scheme illustrated in Figure 2. Where the 1x1 (red) and 2x2 (blue) fragments are positive fragments, and the other two, the 1x2 (yellow) and the 2x1 (green) are negative fragments.

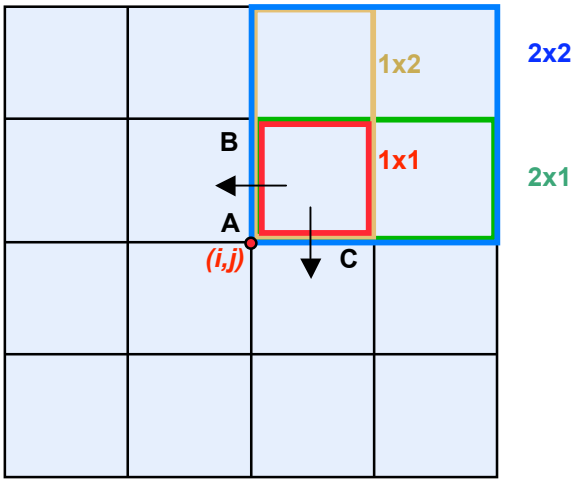

Figure 1. A schematic view of the division of a system into small fragments. This 2D periodic super cell is divided into 4x4 fragment grids. At each fragment grid point *(i,j)*, 4 fragments with different sizes are introduced. Where the red, green, yellow, and blue rectangles represent the fragments of size 1x1, 2x1, 1x2 and 2x2, respectively.

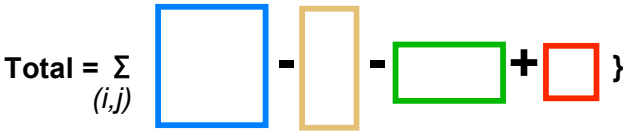

Figure 2. The schematic view of the fragment patching scheme in the LS3DF method for 2D systems. Here the yellow (1x2) and the green (2x1) fragments are negative fragments, and blue (2x2) and red (1x1) are positive fragments.

We can demonstrate how the patching scheme recovers a system. Let's consider the area covered by the red square in Figure 1. For convenience, we denote the fragment 1x1 introduced at the fragment grid point *(i,j)* as $F_{11}(i,j)$. By counting how many positive and negative fragments cover this area, one can easily see whether this area is described properly after all the fragments are added up. This area is covered by 5 positive fragments, they are $F_{11}(i,j)$, $F_{22}(i-1,j-1)$, $F_{22}(i,j-1)$, $F_{22}(i,j)$ and $F_{22}(i-1,j)$. And this area is also covered by four negative fragments, which are $F_{21}(i,j)$, $F_{21}(i-1,j)$, $F_{12}(i,j)$ and $F_{12}(i,j-1)$. When these fragments are summed up using the patching scheme in Figure 2, the red square area will be covered only once after 4 positive and 4 negative fragments cancel out in pairs. We can also show the artificial boundary will be removed in this patching scheme. Let's consider the left boundary of the red square (edge AB). We can define a direction (outward) for this boundary as shown with a left arrow in Figure 1. We can count how many fragments go through this boundary. There are three positive fragments, $F_{11}(i,j)$, $F_{22}(i,j)$, and $F_{22}(i,j-1)$ and three negative fragments, $F_{12}(i,j)$, $F_{12}(i,j-1)$, and $F_{21}(i,j)$. When these six fragments are summed up, the edges from the three negative fragments will cancel out the edges from the other three positive fragments. As a result the edge (AB, outward) will disappear after the fragment summation. Similarly we can see the artificial corners (eg., the corner BAC, outward direction) will cancel out. There are two positive fragments, $F_{22}(i,j)$ and $F_{11}(i,j)$, and two negative fragments, $F_{12}(i,j)$ and $F_{21}(i,j)$. Summing up these four fragments will make the corner BAC disappear.

The patching scheme for 2D systems can be generalized to 3D systems straightforwardly. In 3D cases, at each fragment grid point *(i,j,k)*, eight fragments with different sizes will be introduced, they are 1x1x1, 1x1x2, 1x2x1, 2x1x1, 1x2x2, 2x2x1,2x1x2, and 2x2x2. Among them, 2x2x2, 2x1x1, 1x2x1 and 1x1x2 are positive fragments and 2x2x1, 2x1x2, 1x2x2, and 1x1x1 are negative fragments. And the patching scheme can be expressed in the following form,

$$\text{Total} = \sum_{i,j,k} \{F_{222} + F_{211} + F_{121} + F_{112} - F_{221} - F_{212} - F_{122} - F_{111}\}$$

The presumption of this boundary effect cancellation is that the charge densities of the different fragments at a given boundary will be very similar near that boundary. And our tests have shown that this presumption always holds as long as the smallest fragment (1x1x1) is not too small. For more details about the LS3DF method, see Ref. [8,9].

Figure 3 shows the flow chart of the LS3DF method. In the LS3DF method, the equation to solve is the fragment Khon-Sham equation (as shown in the red box in Figure 3). This can be derived variationally by minimizing the total energy of the whole system with respect to the fragment wavefunctions $\psi_i^F(r)$. This equation is similar to the Kohn-Sham equation in direct LDA methods (LS3DF differs from the direct LDA by

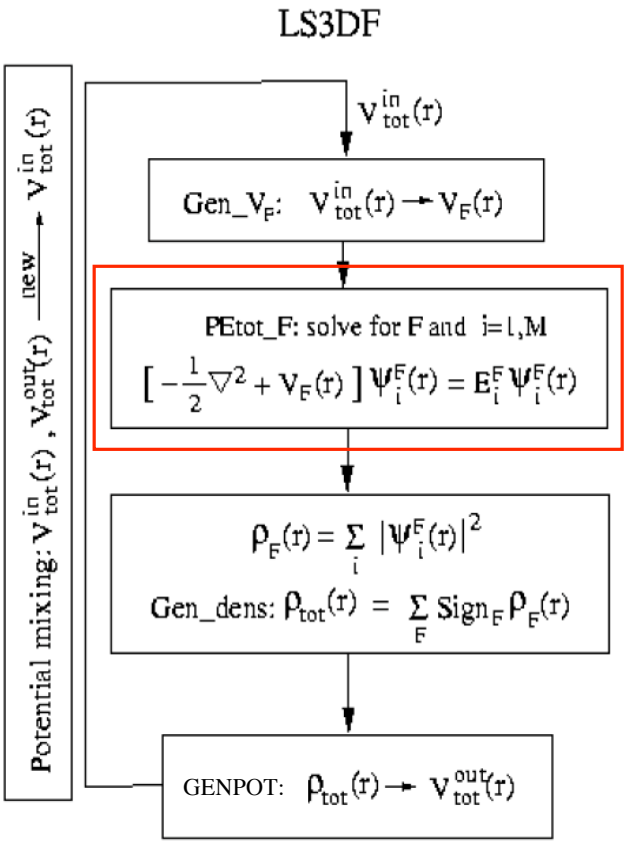

Figure 3. The flowchart of the LS3DF method. The red box shows the Khon-Sham equation for fragments. It is the most time consuming part in the LS3DF code.

only one extra surface passivation potential). But the direct methods solve for the whole system, while the LS3DF method solves for many small systems. As in other direct methods, the equation is solved selfconsistently (SCF) for the whole system. For a given input total potential $V_{tot}^{in}(r)$, the dividing subroutine in the LS3DF code, Gen_V_F, calculates the fragment potential $V_F(r)$ for each fragment. Then the main kernel routine, PEtot_F calculates the wavefunctions for each fragment independently, using one of the iterative eigen

value solvers (eg., conjugate gradient). Then the patching subroutine, Gen_dens, sums up the fragment charge densities to obtain the total charge density of the whole system. From the total charge density, the output total potential V_{tot}^{out} can be calculated by solving the Poisson equation for the whole system using the subroutine, GENPOT. This output total potential V_{tot}^{out} will be the input total potential for the next iteration (in practice, to stabilize the convergence, the V_{tot}^{out} is usually mixed with the input total potentials from the previous iterations before used by the next iteration). These steps will be repeated, until the difference between the output and input total potential is smaller than a predetermined stoping criterion.

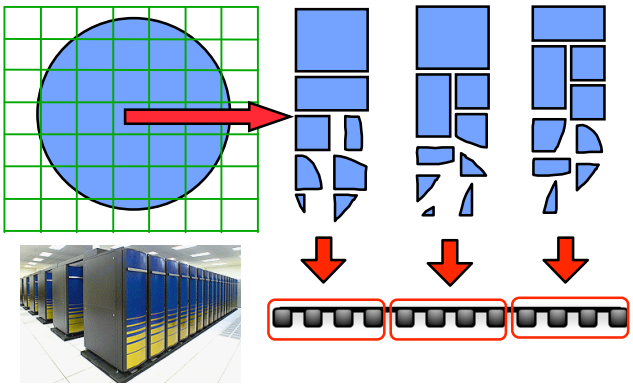

Figure 4. The schematic of the LS3DF calculations.

Figure 4 shows the schematic of the LS3DF calculations. First a large system is divided into many small fragments, and these fragments are sorted into the *Ng* number of groups. The total number of processors is also divided into the same number of processor groups *Ng* with the *Np* number of processors within each group. Then each processor group carries out the calculations for one group of fragments one after another fragments without communication with other processor groups. The ideal parallel scaling of the LS3DF method comes from the minimum communication needed in this most time consuming part.

2.2 Parallel performance and scalability

We have done systematic performance tests for the LS3DF method. We have chosen ZnTe1-xOx (x=3%) alloy super cells with different sizes to perform the strong and weak scaling tests. We carried out these performance tests on Cray XT3 (Franklin, dual core) at NERSC. Figure 5 and 6 show the strong scaling results, where Figure 7 shows the weak scaling tests. In these tests, the time and flops were measured for the second SCF iteration step to avoid possible overhead at the first step. The flops were measured using the profiling tool Craypat 4.1. These results have been reported in Ref. [13]. In Figure 5, the times spent in the four main component subroutines in the LS3DF method are reported. The most time consuming part, PEtot_F scales well to the number of processors, but the other components corresponding the division (Gen_V_F), patching (Gen_dens), and solving the Poisson equation (GENPOT), don't scale. But these parts account for small percentage of the total time (~2%), therefore the overall parallel scaling of the LS3DF (the solid blue line in Figure 6) is almost linear upto more than 17,000 processor cores we tested. Figure 7 shows the efficiency of the code, the sustained performance is around 40% of

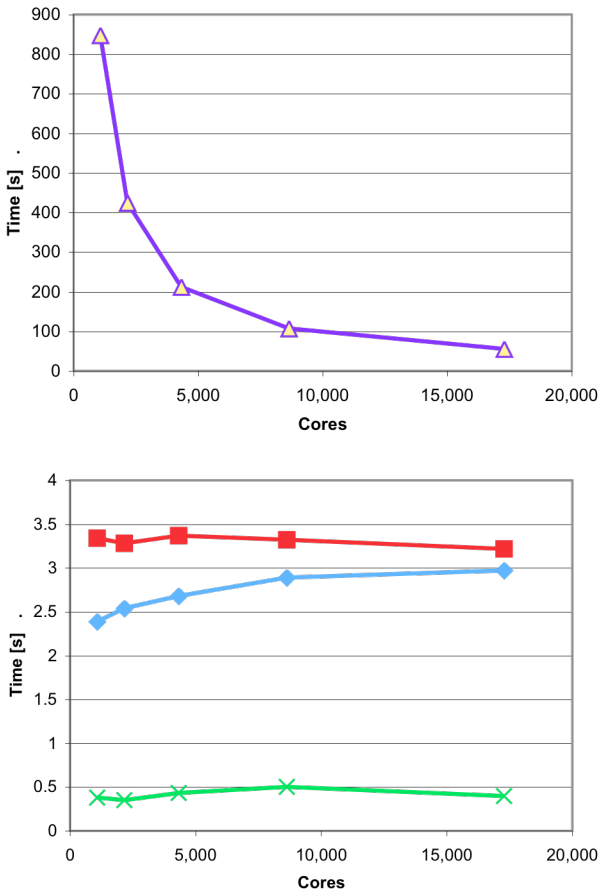

Figure 5. The strong scaling speedups of the four main subroutines in the LS3DF code. The physical system used was $ZnTe_{1-x}O_x$ alloy (x=3%) with 3,456 atoms. The fragment grid size was 8x6x9. These tests are carried out on Cray XT3 (Franklin, dual core) at NERSC.

the peak performance of the Franklin.

We ran our code (with an improved version) on Cray XT4 (Franklin, quad core) at NERSC, Cray XT5 (Jaguar) at NCCS, and Blue Gene/P (Intrepid) at ALCF. The Figure 8 shows the weak scaling results. The LS3DF code has

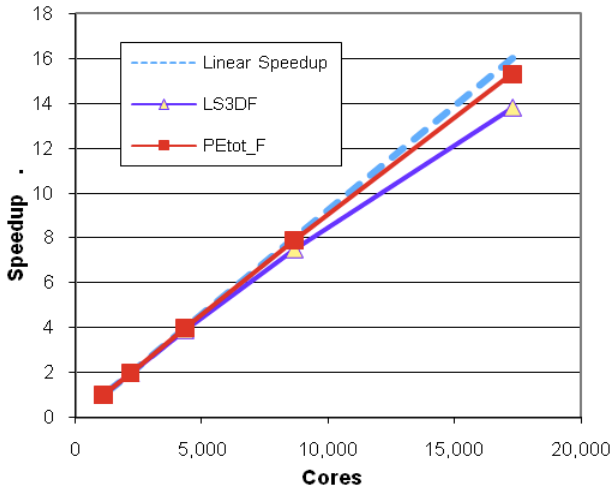

Figure 6. The strong scaling speedups for the LS3DF (blue) and the main routine PEtot_F (red). The dashed line (cyan) is the linear speedup modelled based on Amdah's law. They are the same results as in Figure 5.

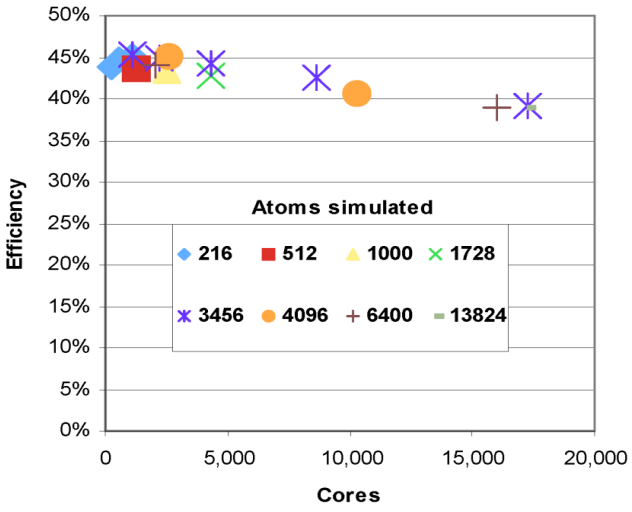

Figure 7. The computational efficiency of the LS3DF method. The systems used were $ZnTe_{1-x}O_x$ alloy (x=3%) with various number of atoms. These are weak scaling tests, and carried out on Cray XT3 (Franklin, dual core).

shown a linear scaling up to the maximum available processors cores on all three supercomputers. It has reached 135 Tflops on 36,864 processors on Cray XT4 (Franklin, quad core) at NERSC at 40% efficiency; 224 Tflops on 163,840 processors on the Blue Gene/P (Intrepid) at ALCF at 40% efficiency; 442 Tflops on 147,456 processors on Cray XT5 (Jaguar) at NCCS at

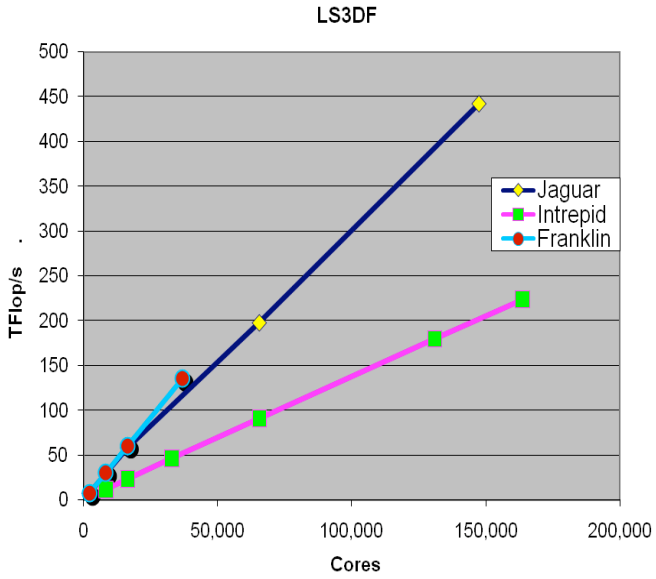

Figure 8. Weak scaling floating point operation rates on different machines. The systems used were $ZnTe_{1-x}O_x$ alloy (x=8%) with various number of atoms.

33% efficiency [10]. In our tests, floating point operations were measured in the double precision.

2.3 Convergence, prefactor and accuracy

As briefly mentioned in the introduction, a common issue in the *O(N)* method is the SCF convergence problem. Figure 9 shows the convergence rate of the LS3DF method, measured by the total energy. To compare with the direct methods, we have chosen a small Si quantum dot with 339 atoms. Compared to the direct methods, there is a slight slowdown with the total energy convergence in the LS3DF method, but there is no convergence problem, and the convergence rate is comparable to the direct methods within 10^{-6} a.u of energy error (the common stopping criteria for SCF iterations). Figure 10 shows the convergence of the LS3DF method, measured by the total potential. For a system with 3456 atoms , within 60 SCF iterations, the difference between the input and output total potentials was reduced to 10^{-2} a.u.

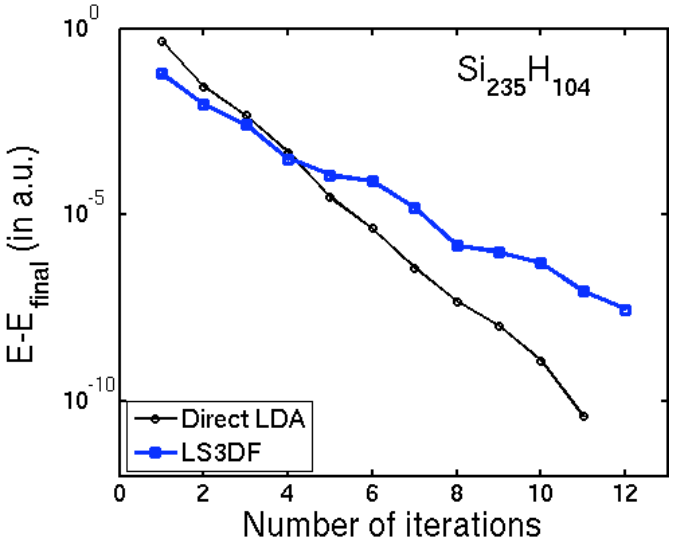

Figure 9. The comparison of the SCF convergence rate measured by the total energy between the LS3DF method (blue) and the direct method (PEtot code).

As seen from the LS3DF patching scheme, one area of the system covered by many different fragments. We have evaluated the prefactor of this method. Figure 11 shows the comparison of the flops needed for the second SCF iteration between the LS3DF method and the direct method (PEtot code). The crossover is at around 550 atoms, this means when the system contains more than 550 atoms, the LS3DF outperforms the direct LDA method. For nano structures with 10,000 atoms, the LS3DF can be faster by 3 orders of magnitude, provided the direct LDA methods can scale up to thousands of processors as the LS3DF method.

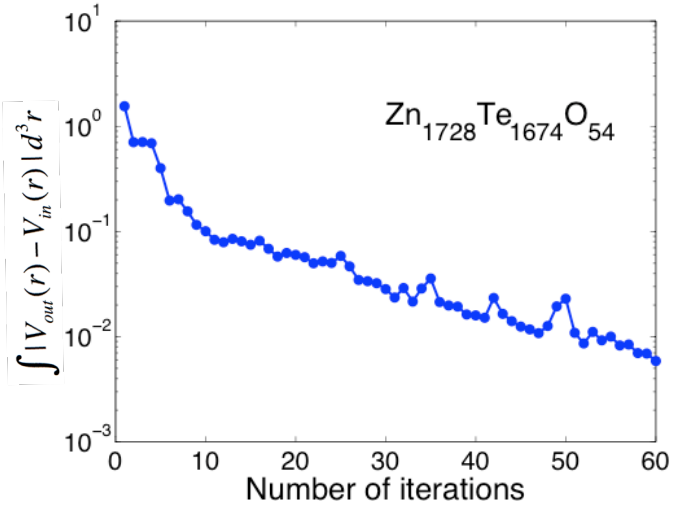

Figure 10. The convergence of the LS3DF method, measured by the total potential (in a.u).

The accuracy of the LS3DF method depends on the size of the smallest fragment (1x1x1 fragment). Usually it is typical to choose 8 atom unit cell as its 1x1x1 fragment. We have evaluated the errors of the total energy, charge density and the dipole moment using Si quantum dots and CdSe quantum rods with a few hundred atoms (so to make the direct calculations possible), and have shown that the error is well under the common stopping criteria in the direct methods [9]. Thus the LS3DF method generates essentially the same results as the direct methods, provided the smallest fragment size (1x1x1) is not too small. In addition, the error of the LS3DF method does not grow with the whole system size, it depends only on the fragment size.

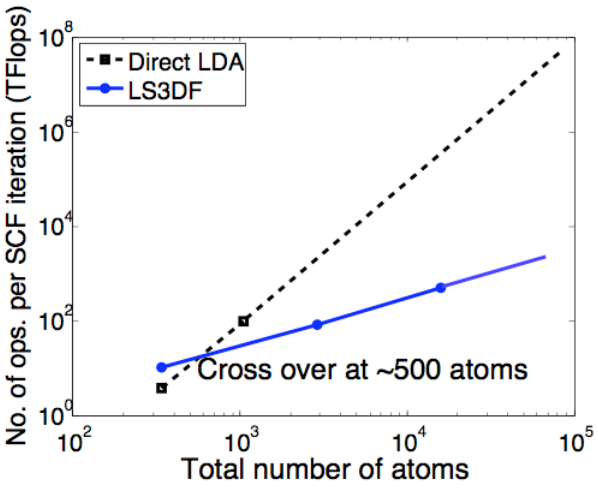

Figure 11. The floating point operations needed for one step SCF iteration in the LS3DF and the direct method (standalone PEtot). The systems used were various size Si quantum dots, and a typical 1 a fragment size (a is lattice constant of Si crystal) was used for the LS3DF calculations. The flops counts were measured on IBM-SP power 3 machine (seabrog) at NERSC, using the profiling tool IPM.

2.4 Summary about LS3DF method

The LS3DF method scales linearly to over 160,000 processors. It reached 442 Tflops. It runs on different platforms with little retuning. The numerical results are the same as a direct DFT based on an $O(N^3)$ algorithm, but at only $O(N)$ computational cost. The LS3DF method can be used to compute electronic structures for >10,000 atom systems with total energy and atomic forces within a couple hours. It can be thousand times faster than the direct LDA calculations.

3. Electronic structure calculations for asymmetric CdSe/CdS core/shell nanorods

3.1 Introduction

With the advance of the synthetic methods, more and more different shapes of nano structures have been synthesized in the labs. Recently Carbone and his colleagues have synthesized asymmetric core/shell structures, using newly developed seed growth method [14]. Their synthesized asymmetric CdSe/CdS core/shell nanorods are illustrated in Figure 12. In the asymmetric core/shell nanorods, a CdSe core (the cyan circle covered area in Figure 12) is embedded in one end of the cylindrical CdS shells.

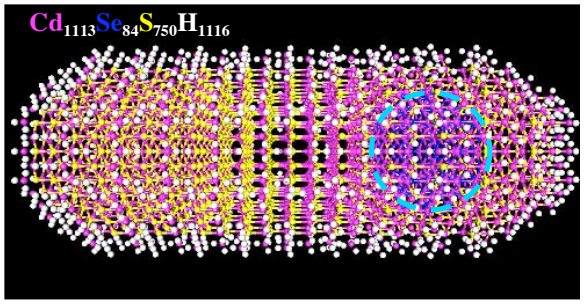

Figure 12. An asymmetric CdSe/CdS core/shell nanorod. A spherical CdSe core (Se:blue) embedded in a CdS cylindrical shell (Cd:magenta; S:yellow). The cyan dashed circle shows the CdSe core area. White dots are pseudo H atoms. The diameters of the cylinder and the core are 2.8 nm and 2.1 nm, respectively. The length of the nanorod is 8.4 nm. There are 3063 atoms in this nanorod. It is constructed as a wurzite structure.

By changing the sizes of the core and the shell (both the diameter and length), one can manipulate the electronic structures inside the nanorods. Hence these nano structures appear to be particularly interesting to solar cell applications. In addition, these asymmetric core/shell structures provide a system on which one can study the quantum confinement effect, the band alignment, the strain (due to the mismatch between the lattice constants of the core/shell semi-conductor materials), and the surface effect. Recently, Luo and Wang have studied the electronic structures of the asymmetric CdSe/CdS core/shell nanorods, using the charge patching method [15], and have predicted the interesting electron and hole localizations [16]. The charge patching method is a non-self consistent method. It constructs the charge density of a large system by carrying out the *ab initio* LDA calculations on a few bulk systems and small surface systems. This method has been used to study many nano structures successfully in the past [17-19]. Nevertheless, since the charge density is obtained non-self consistently, this method might not be sufficient in some cases, e.g., for systems with total dipole moment, or internal electric field. On the other hand, the LS3DF method is perfect in calculating these problems with its selfconsistent charge densities and potentials.

In our present work, we have applied the LS3DF method to the same four CdSe/CdS core/shell nanorods as in Ref. [16]. We have studied the electronic structures of these nanorods, focusing on how the CdSe core and the surface affect the electronic structures inside the system.

3.2 Computational details

We have applied the LS3DF method to four CdS nanorods with/without the CdSe core and with/without surface S atoms. They are CdSe/CdS core/shell nanorods with Cd and Cd+S terminated surfaces, respectively; and the pure CdS nanorods with Cd and Cd+S terminated surfaces, respectively. Where the Cd and Cd+S terminated surfaces are two surface passivation models. In the Cd terminated surface, there are only Cd atoms and pseudo hydrogen atoms (with fractional nuclei charges and the number of electrons) which passivate the surface dangling bonds; while in the Cd+S terminated surface, there are both Cd and S atoms on the surface, in addition to the pseudo hydrogen atoms. These nanorods are all constructed as an ideal wurzite structure, and then relaxed using the valence force field method (VFF) [20]. These nanorods are 8.4 nm long and 2.4 nm in diameter, and have a 2.1 nm of the core diameter when the core exists. There are 3063 atoms in the Cd terminated nanorods, and 2298 atoms in the Cd+S terminated ones.

Figure 13 shows how a CdSe/CdS core/shell nanord was divided into small fragments (using the CdSe/CdS core/shell nanorod with the Cd terminated surface as an example). Where (a) is the (orthogonal) side view of the nanorod, and (b) is a cross section which passes the core area. The solid red lines in (a) and (b) represent the real space numerical grid box that contains the nanorod, and the green arrows represent the directions of c-axis and two primitive lattice vectors, ***a*** and ***b***. The dashed cyan circle covers the core region. As shown with the dotted red lines, the nanorod was cut into a 24x5x5 fragment grid, along the direction of c-axis and the two primitive lattice vectors, ***a*** and ***b***. And the size of the 1x1x1 fragment is (1/2c)x(2a)x(2b), where a=b=4.288A, c=7.002A. And the number of atoms in a 1x1x1 fragment ranges from 3 to 72. The maximum number of atoms in a

2x2x2 fragment is 257 (including about 150 surface passivation pseudohydrogen atoms)

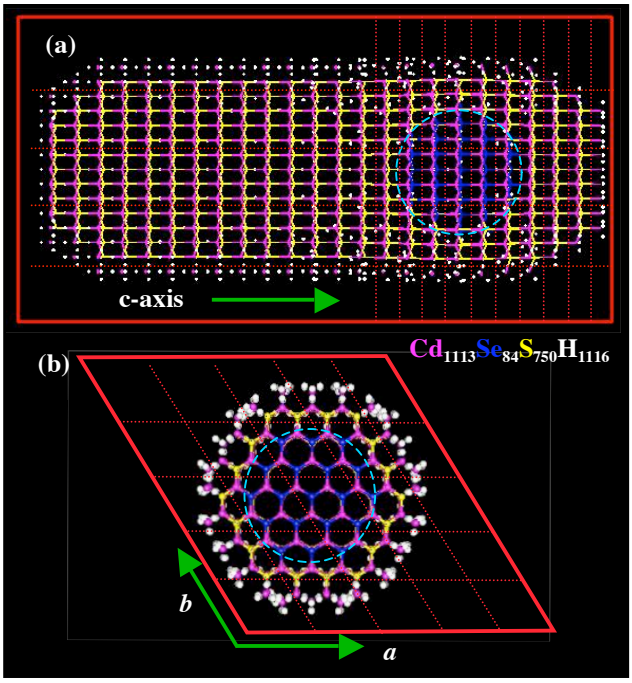

Figure 13. This figure shows how we divide the CdSe/CdS nanorod into small fragments. Where (a) is the (orthogonal) side view of the nanorod, and (b) is a cross section which passes the core area. As shown in the dotted red lines, the nanorod is cut into a 24x5x5 fragment grid. The solid red lines in (a) and (b) represent the real space numerical grid box that contains the nanorod, and the green arrows represent the directions of the c-axis and two primitive lattice vectors, ***a*** and ***b*** of this wurzite structure. The dashed cyan circle covers the core region. The color of each atom is the same as in Figure 12.

We used 48, 24, and 24 numerical grid points (in real space) in one unit length of the c-axis and the other two primitive lattice vectors to describe the wave functions and charge densities. A cut off energy of 35 Ry was used for all fragment calculations. The surface passivation potential was generated by an initial selfconsistent calculations for each fragment. The total of 60 SCF iterations have been carried out in all four nanorods calculations. The total computation time was ~ 3 hours for each nanorod.

Figure 14 and 15 show the SCF convergence rates of the total energy and the total potential in two core/shell nanorods calculations, respectively. Within 60 SCF iterations, the total energy was reduced to < 10^{-5} a.u., and the total potential error was reduced to ~10^{-3} a.u. We have

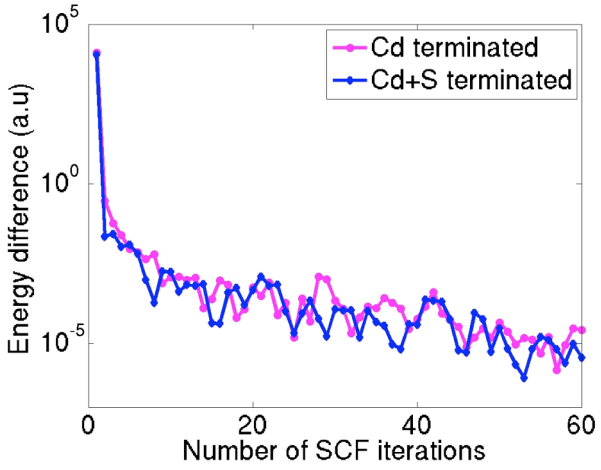

Figure 14. The convergence of the LS3DF method, measured by the total energy for the CdSe/CdS core/shell nanorods with two different surface passivations Cd terminated (magenta) and Cd+S (blue) terminated.

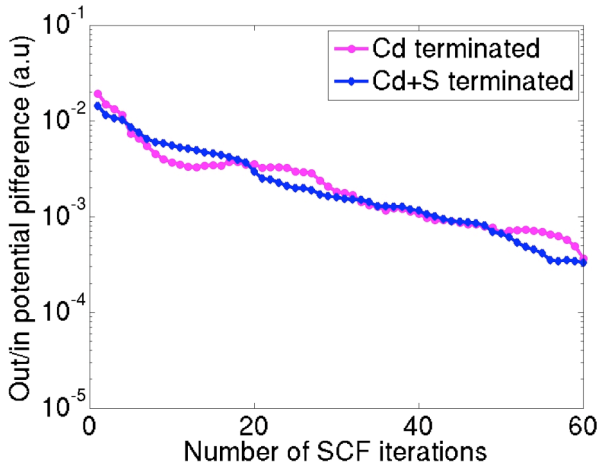

Figure 15. The convergence of the SCF iterations, measured by the total potential for the CdSe/CdS core/shell nanorods with two different surface passivations Cd terminated (magenta) and Cd+S (blue) terminated.

seen the similar convergence rate in the other two pure CdS nanorods calculations as well (not shown in the figure).

The direct outputs from the LS3DF code are the total potential (or the charge density) and the total energy. To calculate the band edge states, the valence band maximum (VBM, or hole) and the conduction band minimum

(CBM, or electron) states, the folded spectrum method (escan code) [20] needs to be applied, using the total potential obtained from the LS3DF calculation as the input. The folded spectrum method allows one to calculate the electron wavefunctions in the small energy window of interest within an *O(N)* computational cost. The band-corrected pseudo potential [18] was used, and the same cut off energy (35 Ry) and the real space numerical grids were used as in the LS3DF calculations.

3.3 Results and discussion

Table 1 shows the band gaps of the four nanorods. We can see how the band gap changes with different surfaces (rows 2, and 3) and with the introduction of the CdSe core in the CdS nanorods (columns 2, and 3). Table 1 shows that the band gap change due to the different surface passivations (~0.06eV) is smaller than that due to the introduction of the CdSe core (~0.15eV) inside the CdS nanorods. Figure 17 illustrates the VBM and CBM energy level changes when the CdSe core and the different surface passivation models are introduced. The band gap difference between the CdS nanorods with/without the CdSe core is mainly from the VBM shift, the CBM change is negligible. The different surface passivations make the CBM and VBM shift together.

Surface / nanorod	Cd termin. (eV)	Cd+S termin. (eV)	Band gap change (eV)
Pure CdS	2.2174	2.2613	**0.0439**
CdSe/CdS core/shell	2.0534	2.1299	**0.0765**
Band gap change (eV)	**-0.1640**	**-0.1314**	

Table 1. The band gaps of the four CdS nanorods with/without the CdSe core, and with the Cd terminated/Cd+S terminated surfaces. The 4-th column and the 4-th row show the band gap differences of the columns 3 and 2 (column3 – column2) and of the row 3 and 2 (row3 –row2), respectively.

Table 2 shows the calculated dipole moments for the four nanorods. None zero dipole moments inside the nanorods indicate that there exist the internal electric filed inside these nanorods. The dipole moment change due to the different surface passivations is significant in the pure CdS rods (row 2). As one can see from the table, the dipole moment along the c-axis, dz (the other two components, dx and dy, are small) has different signs in the two different surface passivation models. This

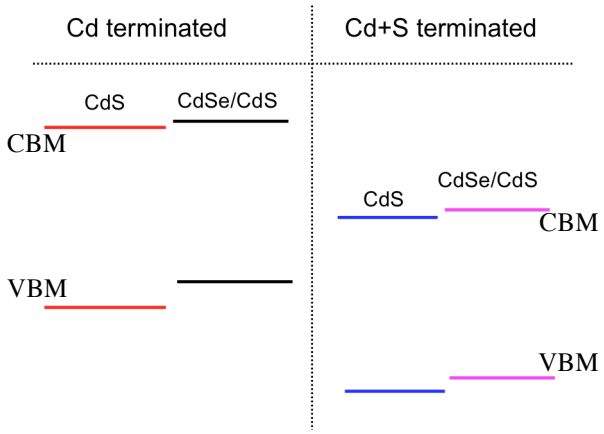

Figure 17. The illustration of the VBM and CBM energy level changes when the CdSe core are introduced in the CdS nanorods and two different surface passivation models are used. Where the red, and black are for the CdS and CdSe/CdS coreshell nanorods with the Cd terminated surfaces, respectively, while the blue and magenta are for the CdS and CdSe/CdS core/shell naorods with Cd+S terminated surfaces, respectively.

indicates that one can change the direction of the internal electric field inside the pure CdS nanorods by manipulating its surface. But in the CdSe/CdS core/shell nanorods, the effect from the surface is not as significant as in the pure CdS nanorods (row 3).

Surface / nanorod	Cd termin. (a.u)	Cd+S termin. (a.u)	Dipole moment change (a.u.)
Pure CdS	0.0070, 0.1590, **6.6616**	-0.0364, -0.0586, **-6.0208**	-0.0434 -0.2176 **-12.6824**
CdSe/CdS core/shell	-0.0100, 0.1298, **-8.6135**	-0.0064, -0.0456, **-10.6354**	0.0036 -0.1754 **-2.0219**
Dipole moment change (a.u)	-0.0170 -0.0292 **-15.2751**	0.0300 0.0130 **-4.6146**	

Table 2. The calculated dipole moments (dx,dy,dz) of the four CdS nanorods, where the z axis aligns with the c-axis, and the dz is in bold blue. The 4-th column and the 4-th row show the component-wise differences of the columns 3 and 2 (column 3 –column 2) and of the row 3 and 2 (row 3 –row2), respectively.

Figure 18 shows the isosurface of the wave function square (charge density) of the VBM (hole) and the CBM (electron) states for the four nanorods. In the both surface passivation models, the electron (CBM) and hole (VBM) states of the CdSe/CdS core/shell nanorods are separated. The electron states are localized in the center of the rods.

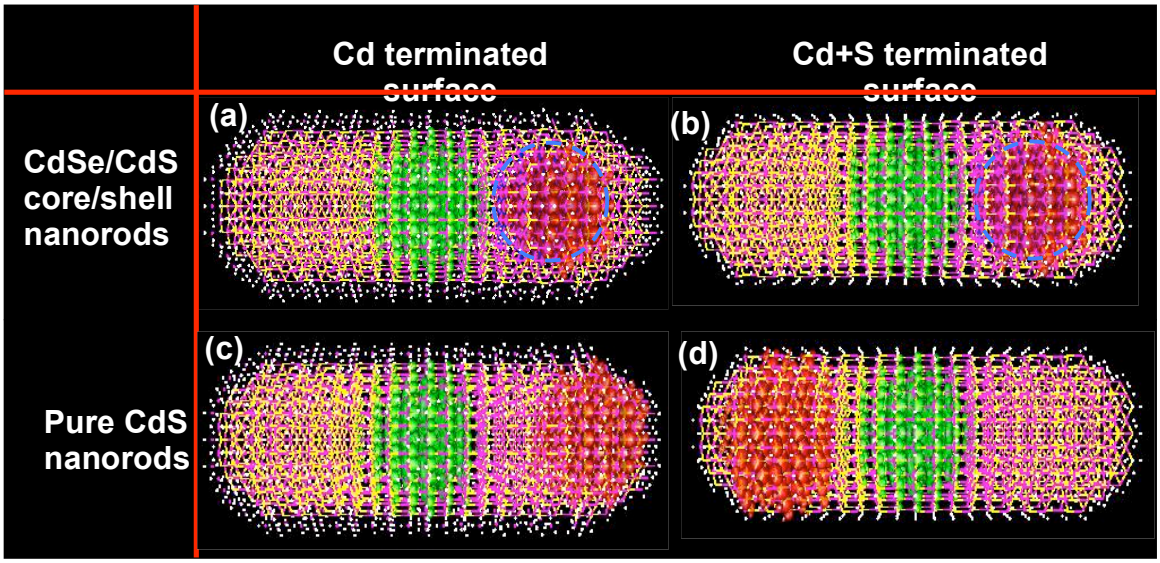

Figure 18. Isosurface of the wave function square of the conduction band minimum (CBM, green) and the valance band maximum (VBM, red) states of the four CdS nanorods with/without CdSe core. Where (a) and (b) are for the CdSe/CdS core/shell nanorods with the Cd terminated and the Cd+S terminated surfaces, respectively, while (c) and (d) are for the pure CdS nanorods with the Cd terminated and the Cd+S terminated surfaces, respectively. The isovalue larger than 0.001 e/bhor^3 was shown for both VBM and CBM

The hole (VBM) states are localized in core area. The surface significantly changes the hole state localization in the pure CdS nanorods. In the Cd terminated pure CdS nanorod, the hole state (red) is localized at the right end of the rod, while in Cd+S terminated surface model, the hole state is localized in the left end of the rod. The CdSe core inside the asymmetric core/shell nanorods seems to play a dominant role to control the spatial location of the hole localization. This could be a useful feature for the electronic device design, since we can control where to localize the hole while we don't have an exact knowledge about the surface passivation in reality.

3.4 Summary about CdSe/CdS core/shell calculations

We have applied the LS3DF method to the asymmetric CdSe/CdS core/shell nanorods with different surfaces, and also to their counterparts, the pure CdS nanorods to study how the core and the surfaces affect the electronic structures in these nanorods. We have calculated the dipole moments of these nanorods, and have calculated the VBM (hole) and CBM (electron) states and the band gaps, utilizing the folded spectrum method. We have observed that the hole states are localized in the CdSe core area, and the electron states are localized in the center area of the nanorods for both the surface passivation models (Cd terminated and Cd+S terminated). The introduction of the CdSe core in the CdS nanorods, makes the band gaps decrease by 0.15 eV and this change was mainly due to the VBM shifts (up). We also observed that the surfaces have significant effects to the hole state localizations and dipole moments in the pure CdS nanorods. But with the presence of the CdSe core in the nanorod, the effect of the surfaces seems to be suppressed. We have seen that the core plays a dominant role in determining the spatial locations of the hole localization, and also the direction of the internal electric filed inside the asymmetric core/shell nanorods.

We would like to point out that our study is a preliminary result for a given nanorod size. Since the electronic structure strongly depends on their sizes, more systematic study on the core/shell nanorods with different sizes (core/shell diameters, and the length of nanorods),

especially at more reality relevant sizes, is needed to conclude how the core and surface affect the electronic structures inside these nanorods. In this study, we calculated the nanorods with the same sizes as in Ref. [16], which is ~2 times smaller than the smallest core/shell naorods synthezied in the labs.

Conclusion

We have presented the LS3DF method for *ab initio* electronic structure calculations. We have described how the method works without going into the implementation details, and have presented the parallel and algorithmic scalings, and have summarized the accuracy and the SCF convergence rate. We have demonstrated how this method can be used to study the electronic structures of large nano systems. As a summary, the LS3DF method is an *O(N)* ab initio electronic structure code ; it scales linearly to hundreds of thousands of computer processors; it yields essentially the same results as the direct LDA methods; it can solve a nano system with thousands of atoms selfconsistently in a couple of hours.

Since the code is newly developed, there are still many features need to be implemented to make it more stable and with more functionalities.. Nevertheless, as it is now, it can be applied to study the electronic structures of large systems containing tens of thousands of atoms. We expect it will find wide applications Nanostructure calculations.

Acknowledgments

The authors would like to thank Ying Luo at Beijing Normal University for providing the VFF relaxed CdSe/CdS core/shell and CdS nano structures and the band gap corrected pseudo potential for sulfide. And Zhao would like to thank Byounghak Lee for his help with running the folded spectrum code (escan). This work was supported by the ASCR Office in the DOE, Office of Science, under contract number DE-AC02-05CH11231. This work was also supported by the BES office of the DOE, Office of Science, under LAB03-17 initiative, contract No. DE-AC02-05CH11231. It is supported by the DOE INCITE project. It used the resources of National Energy Research Scientific Computing Center (NERSC). It also used the resources of National Center for Computational Sciences (NCCS), and Argonne Leadership Computing Facility (ALCF).

About the Authors

Zhengji Zhao is a HPC consultant at NERSC at Lawrence Berkeley National Laboratory (LBNL). She supports chemistry and materials science applications at NERSC. She can be reached by email ZZhao@lbl.gov and by phone 510-495-2540. Lin-Wang Wang is a staff scientist at computational research division at Lawrence Berkeley National Laboratory. His research interest is the methodology development in electronic structure calculations. He can be reached by email LWWang@lbl.gov and by phone 510-486-5571.

References

[1] F. Gygi and E. Draeger and B. R. de Supinski and R. K. Yates and F. Franchetti and S. Kral and J. Lorenz and C. W. Ueberhuber and J. Gunnels and J. Sexton, Proceedings of the 2005 ACM/IEEE Conference on Supercomputing, (2005).

[2] G. Goedecker. Linear scaling electronic structure methods. Rev. Mod. Phys, 71:1085, 1999.

[3] G. Galli, M. Parrinello, Phys. Rev. Lett. **69**, 3547 (1992).

[4] J.-L. Fattebert and F. Gygi, Phys. Rev. B **73**, 115124 (2006).

[5] X.P. Li, R.W. Nunes, D. Vanderbilt, Phys. Rev. B **47**, 10891 (1993).

[6] D.R. Bowler, R. Choudhury, M.J. Gillan, T. Miyazaki, phys. stat. sol. b **243**, 989 (2006).

[7] W. Yang, Phys. Rev. Lett. **66**, 1438 (1991).

[8] Lin-Wang Wang, Zhengji Zhao, and Juan Meza,, Phys. Rev. B 77, 165113 (2008).

[9] Zhengji Zhao, Lin-Wang Wang, and Juan Meza, J. Phys.: Condens. Matter **20** (2008) 294203.

[10] Zhengji Zhao, Juan Meza, Byounghak Lee, Hongzhang Shan, Eric Strohmaier, and David Bailey, and Lin-Wang Wang, a special issue of the Journal of Physics Conference Series, SciDAC (2009).

[11] W. Kohn, Phys. Rev. Lett. **76**, 3168 (1996).

[12] http://hpcrd.lbl.gov/ linwang/PEtot/PEtot.html

[13] Lin-Wang Wang, Byounghak Lee, Hongzhang Shan, Zhengji Zhao, Juan Meza, Erich Strohmaier, David Bailey, Linearly Scaling 3D Fragment Method for Large-Scale Electronic Structure Calculations, Gordon Bell submission, (2008).

[14] Luigi Carbone Concetta Nobile Milena De Giorgi, Fabio Della Sala, Giovanni Morello, Pierpaolo Pompa, Martin Hytch, Etienne Snoeck, Angela Fiore, Lsabella R. Franchini, Monica Nadasan et.al. 2007 7(10) 2942-2950, Nano Lett.

[15] L.W. Wang, Phys. Rev. Lett. **88**, 256402(2002)

[16] Ying Luo, Lin-Wang Wang, Electronic Structures of the nanorod with CdSe/CdS core-shell structure, to be submitted.
[17] L.W.Wang and J.Li, Phys. Rev. B **69**, 153302 (2004).
[18] J. Li and L.W.Wang, Phys. Rev. B **72**, 125335 (2005).
[19] J. Schrier and L.W.Wang, Phys. Rev. B **73**, 245332 (2006).
[20] C. Pryor, aJ.Kim, L.W.Wang, A.J.Williamson, and A.Zunger, J. Appl. Phys. **83**, 2548 (1998)
[21] L.W. Wang and A.zunger, J. Chem. Phys. **100**, 2394 (1994).